

Current instability and diamagnetism in small-diameter carbon nanotubes

J. González

Instituto de Estructura de la Materia. Consejo Superior de Investigaciones Científicas. Serrano 123, 28006 Madrid. Spain.
(April 14, 2024)

We investigate the electronic instabilities in carbon nanotubes of short radius, looking for the breakdown of the Luttinger liquid regime from the singular behavior of the charge stiffness at low energies. We show that such a breakdown is realized in the undoped (3,3) nanotubes through the onset of phase separation into regions with opposite electronic current. The phenomenology derived from this regime is consistent with the formation of a pseudogap in the single-particle spectrum as well as with a divergent diamagnetic susceptibility, as observed in the experiments carried out in carbon nanotubes of small diameter.

71.10.Pm, 73.22.Gk, 73.63.Fg

Carbon nanotubes (CN) are among the best candidates for the development of devices in molecular electronics. For this reason, there has been great interest during the last years in the investigation of their electronic properties. As the electrons are constrained to move in the reduced dimensions of the tube, CN constitute a paradigm of strongly correlated electron system [4]. Thus, it has been possible to observe signatures of Coulomb blockade in short nanotube samples, as well as signatures of 1D transport characteristic of Luttinger liquid behavior [5,6].

Yet there has been also clear evidence of superconducting (SC) correlations in CN attached to suitable contacts [7,8]. Supercurrents have been observed in the samples with SC electrodes reported in Ref. [7], providing evidence of the proximity effect in the CN [9]. Moreover, SC transitions have been measured in nanotube ropes attached to highly transparent contacts [10]. More recently, measurements carried out in CN inserted in a zeolite matrix have supported the conclusion that strong SC correlations should exist in CN of very short diameter, leading to a transition temperature $T_c \sim 15$ K [11].

The experiment reported in Ref. [11] has provided evidence of the diamagnetic behavior of the CN at low temperatures. From inspection of the I-V characteristics, it has been also appreciated the appearance of a gap in the single-particle spectrum, which has been used to infer the value of T_c [11]. However, the lack of evidence for a true SC transition stresses the fact that the mentioned observations refer to properties of the individual CN, which cannot be coupled by electron hopping as they only have a weak interaction with the zeolite walls [11]. In general, the tunneling amplitude between metallic nanotubes is what dictates the setting of 3D Cooper-pair coherence and the value of T_c [12,13]. The existence of a low-energy scale intrinsic to the individual CN demands therefore a reexamination of the role of the dominant correlations in nanotubes of short radius.

The nanotube diameter $d = 4.2 \pm 0.2$ Å reported in Ref. [11] is closer to the value calculated for a (3,3) nanotube geometry, although the presence of (5,0) nanotubes in

the zeolite matrix cannot be discarded [14]. It has been shown by using the local-density functional method that the (3,3) nanotubes have the same band structure of typical armchair nanotubes near the Fermi level, with a pair of subbands crossing at two opposite momenta [14]. The case of the (5,0) nanotubes is different in that they have one more subband crossing the Fermi level, with angular momentum $L = 0$ in the zigzag geometry. We will show that the (5,0) nanotubes have an extended low-energy phase with strong charge-density-wave (CDW) correlations, while the dominant low-energy instability for the (3,3) geometry is given by the phase separation into regions with opposite electronic current [15]. We will see that this is consistent with the existence of a low-energy transition inherent to the individual CN, allowing also to account for the phenomenology reported in Ref. [11].

Focusing first on the (3,3) nanotubes, the interaction processes between different low-energy branches crossing at Fermi points k_F and k_F can be classified by attaching to them respective coupling constants $g_i^{(j)}$ [16]. The lower index discerns whether the interacting particles shift from one Fermi point to the other ($i = 1$), remain at different Fermi points ($i = 2$), or they interact near the same Fermi point ($i = 4$). The upper label follows the same rule to classify the different combinations of left- and right-movers, including the possibility of having Umklapp processes ($j = 3$) in the undoped system.

We will adopt in what follows a bosonization approach to deal with the interactions in forward-scattering (FS) channels, while the effect of the rest of interactions will be considered through the analysis of their low-energy scaling. Thus, we first introduce an electron density operator $\rho_{ri}(k)$ for each of the linear branches of the subbands crossing the Fermi level, where the index $r = L, R$ denotes the left- or right-moving character and the index $i = 1, 2$ labels the Fermi point. It becomes possible to decouple the FS channels by passing to the combinations

$$\rho_r(k) = \begin{pmatrix} \rho_{r1}(k) & \rho_{r2}(k) \end{pmatrix} = \frac{P}{2} \quad (1)$$

where $P = 1; +1$ for $r = L, R$, respectively. The Hamiltonian for the FS interactions can be written in terms of

elds $\phi_s(\mathbf{x})$, such that $\phi_s(\mathbf{x}) = \phi_L(\mathbf{x}) + \phi_R(\mathbf{x})$, and their conjugate momenta $\pi_s(\mathbf{x})$:

$$H_{FS} = \frac{1}{2} \sum_s \int d\mathbf{x} \left[v_{Js} (\pi_s(\mathbf{x}))^2 + v_{Ns} (\phi_s(\mathbf{x}))^2 \right] \quad (2)$$

The four independent velocities are given by

$$v_J = v_F + (1 - \frac{1}{K}) g_4^{(4)} g_2^{(4)} (g_2^{(2)} g_4^{(2)}) \quad (3)$$

$$v_N = v_F + (1 - \frac{1}{K}) g_4^{(4)} g_2^{(4)} + (g_2^{(2)} g_4^{(2)}) \quad (4)$$

where v_F is the Fermi velocity. In terms of these quantities, the renormalized velocities of the liquid are $u = \frac{v_F}{v_N}$, while the charge stiffnesses are $K = \frac{v_F}{v_N} = v_N$ [17].

In general, the significance of the interactions is given by their scaling behavior at low energies. The scaling equations of the $g_i^{(j)}$ couplings have been obtained in Ref. [16] for an arm chair geometry. Here we improve nonperturbatively the equations writing the scaling dimensions in terms of the K parameters, and we introduce the pertinent modifications for the (5,0) geometry. The new equations read:

$$\frac{\partial g_1^{(1)}}{\partial l} = \frac{1}{v_F} (g_1^{(1)} g_1^{(1)} + g_1^{(2)} g_2^{(1)}) - \frac{1}{v_F} u_F u_B \quad (5)$$

$$\frac{\partial g_1^{(2)}}{\partial l} = (1 - \frac{1}{K}) g_1^{(2)} + \frac{1}{v_F} (g_4^{(3)} g_1^{(3)} - g_2^{(1)} g_1^{(1)} - (2)(u_F^2 + u_B^2)) \quad (6)$$

$$\frac{\partial g_2^{(1)}}{\partial l} = (1 - \frac{1}{K}) g_2^{(1)} + \frac{1}{v_F} (g_4^{(1)} g_1^{(2)} - 2g_4^{(1)} g_2^{(1)} + g_4^{(3)} g_1^{(3)} - g_4^{(3)} g_2^{(3)} - g_1^{(2)} g_1^{(1)} - u_F u_B) \quad (7)$$

$$\frac{\partial g_1^{(3)}}{\partial l} = (1 - K_+) g_1^{(3)} + \frac{1}{v_F} (2g_1^{(3)} g_1^{(1)} + g_2^{(3)} g_1^{(1)} + g_4^{(3)} g_1^{(2)}) \quad (8)$$

$$\frac{\partial g_2^{(3)}}{\partial l} = (1 - K_+) g_2^{(3)} + \frac{1}{v_F} (g_4^{(1)} g_1^{(3)} - 2g_4^{(1)} g_2^{(3)} + g_4^{(3)} g_1^{(2)} - g_4^{(3)} g_2^{(1)}) \quad (9)$$

$$\frac{\partial g_4^{(3)}}{\partial l} = (2 - K_+ - \frac{1}{K}) g_4^{(3)} + \frac{1}{v_F} (g_4^{(3)} g_4^{(1)} - 2g_2^{(3)} g_2^{(1)} + g_1^{(3)} g_2^{(1)} + g_2^{(3)} g_1^{(2)} + g_1^{(3)} g_1^{(2)}) \quad (10)$$

where l stands for minus the logarithm of the energy (temperature) scale measured in units of the high-energy scale E_c of the 1D model (of the order of 0.1 eV). The $g_i^{(j)}$ couplings only arise in the (3,3) nanotubes without doping (which is the likely experimental condition when embedded in the insulating zeolite matrix) and the u_F and u_B couplings (to be defined later) apply only to the (5,0) nanotubes. The rest of equations not written here retain the expressions given in Ref. [16].

The scaling equations have to be solved with initial conditions accounting for the competition between the Coulomb interaction and the effective interaction arising from phonon-exchange [18]. The latter turns out to be attractive in the backscattering (BS) channels and repulsive in the Umklapp channels [12,19]. Its effective coupling g has a strength $0.3 - 0.9$ times $v_F = n$ for a (n,n) nanotube [19]. This is comparable to the strength of the Coulomb interaction in BS and Umklapp processes, which we have taken as $0.2 e^2 = n$ following Refs. [2] and [3]. Given that $e^2 = 2/7v_F$, the Coulomb repulsion only becomes dominant in forward-scattering processes mediated by the potential $V(q) = (2e^2/\epsilon) \log(1 + q_0/q)$, where q is the momentum and ϵ a suitable dielectric constant [20]. Under these initial conditions, the scaling equations develop an unstable flow below certain energy scale, at which the $g_2^{(1)}$ and $g_4^{(1)}$ couplings enter a regime of large attraction while the $g_4^{(2)}$ and Umklapp couplings are driven towards large repulsion in the (3,3) nanotubes.

We have discerned the character of the electronic instability by looking for the susceptibility with the fastest growth as $l \rightarrow 1$, as well as for the possible breakdown of the Luttinger liquid parameters K . We have checked that this latter instance takes place before any CDW or pairing response function starts to diverge in the (3,3) nanotubes. Their phase diagram is represented in Fig. 1. The strength of the Coulomb potential V for the samples reported in Ref. [11] has to be determined taking into account the screening effects from the large 3D array of CN inserted in the zeolite channels. These effects can be studied by generalizing the many-body approach devised in Ref. [21]. Thus, by performing a RPA analysis incorporating the electrostatic coupling between all the CN in the array, we have found that the Coulomb potential ranges from $V = 0.5 e^2$ at $q = 10 \text{ nm}^{-1}$ to a saturation value $V = 0.9 e^2$ for $q = 0.1 \text{ nm}^{-1}$. Taking $e^2 = 2/7v_F$ and $|j_j| = 0.2 - 0.3 v_F$ for the (3,3) nanotubes, we observe that the relevant regime corresponds to the phase $K_+ = 0$, with very weak SC or CDW correlations.

The vanishing of the K_+ parameter corresponds to an instability in the balance between left- and right-moving electrons in the system. This follows from the fact that the vanishing of v_{J+} in (3) is what triggers the instability. A phase with $K_+ = 0$ has been already described in the study of CN with purely repulsive interactions [4]. This instance has been also analyzed in Ref. [22]. In the case of CN of short radius, however, we have a nonnegligible strength of the phonon-exchange interaction. This leads to a different physical situation as the velocity v_{J+} remains finite, and the compressibility $K_+ = u_+$ is nonvanishing at the point of the transition. We will see that the vanishing of v_{J+} marks actually the divergence of the K_+ correlations, opening a regime of phase separation into regions with opposite electronic current.

The onset of the phase characterized by the vanishing

of K_+ explains the apparent gap that has been measured from the I-V curves in Ref. [11]. The development of the gap shown in Fig. 2 of that Reference takes place through the change in the functional form of the I-V characteristics as the temperature is lowered, resembling the behavior of a power-law dependence with increasing exponent. The same kind of behavior has to be found in the differential conductance dI/dV , which gives a measure of the density of states near the Fermi level.

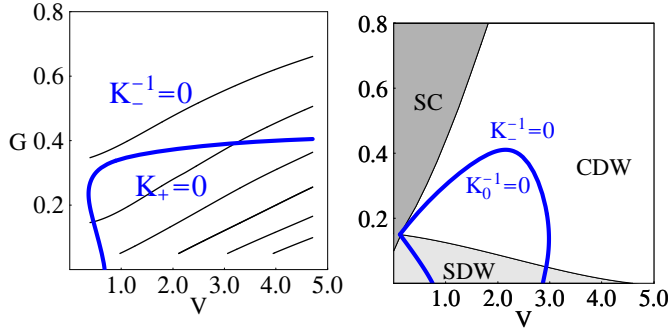


FIG. 1. Phase diagram of (3,3) (left) and (5,0) (right) CN, in terms of the Coulomb potential V (in units of v_F) and the effective coupling of the phonon-exchange interaction $G = 4\gamma\gamma_F v_F$. The thick lines are boundaries between the different phases characterized by the breaking of the parameters K_+ and K_0 at low temperature scales. In the (3,3) nanotubes, CDW correlations at zero momentum are dominant at the singular point, but with low strength represented by the contours of constant CDW response function $R = 2; 4; 8; 16; 32; 64$ (from top to bottom). For the (5,0) nanotubes, three different regimes arise with strong correlations at the singular point of K_+ or K_0 , given by the dominance of the $2k_F$ CDW (white area), the $2k_F$ spin-density-wave (light area), or the s-wave SC response function (dark area).

In our description, the depletion of the density of states n'' near the Fermi level can be evaluated with the usual bosonization methods, with the result that

$$n'' \propto (K_+ + 1)(K_+ + K_- + 1)(K_0 + 4) = 8 \quad (11)$$

The density of states follows a power-law behavior with an increasingly large exponent as K_+ vanishes in the low-temperature limit, as represented in Fig. 2. The plots in the figure show the development of the pseudogap at low temperatures. We observe that the shapes of the curves obtained from (11) are in very good agreement with the form of the I-V characteristics reported in Ref. [11].

Shifting now to the case of the (5,0) nanotubes, their behavior can be studied by making the parallel of the above analysis. One has to incorporate an additional type of density operators for the subband with angular momentum $L = 0$ (and Fermi velocity v_F^0), which has its own renormalized velocity u_0 and charge stiffness K_0 . Moreover, there are new interaction processes in which

one or two of the incoming modes belong to the subband with $L = 0$. These interactions may be classified with an additional set of couplings $f_i^{(j)}$, where the indices i and j keep the same meaning as for the $g_i^{(j)}$ couplings. Finally, there may be processes in which two particles with opposite L around the Fermi points 1 and 2 end up in the subband with $L = 0$, requiring the introduction of new couplings u_F and u_B , for the respective cases with and without change of chirality of the particles.

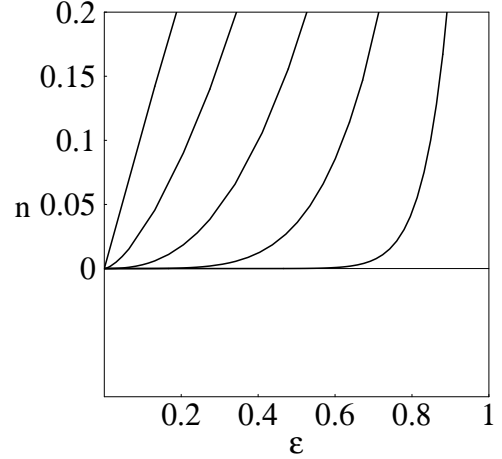


FIG. 2. Plot of the density of states n'' for $V = 0.75 v_F$ and $4\gamma\gamma_F v_F = 0.2$. The curves correspond to values of m minus the logarithm of the temperature scale $l = 3.21; 3.225; 3.232; 3.235$ and 3.236 .

The processes given by the couplings u_F and u_B have been overlooked in other analyses of the (5,0) nanotubes [23], while they are determinant in the enhancement of the SC correlations. Their scaling equations are given by

$$\begin{aligned} \frac{\partial u_F}{\partial l} &= u_F - \frac{1}{2 v_F} (g_1^{(2)} u_F + (g_2^{(1)} + g_1^{(1)} + f_4^{(1)}) u_B) \quad (12) \\ \frac{\partial u_B}{\partial l} &= u_B - \frac{1}{2 v_F} (g_1^{(2)} u_B + (g_2^{(1)} + g_1^{(1)} + f_4^{(1)}) u_F) \\ &\quad + \frac{f_1^{(1)}}{v_F} (u_F - 2 u_B) \quad (13) \end{aligned}$$

where $\epsilon = 1 - 1/(4K_+)$, $\epsilon = 1/(4K_-)$, $\epsilon = 1/(2K_0) + f_2^{(2)}/v_F$, $\epsilon = v_F/v_F^0$ and $\epsilon = 2/(1 + v_F^0/v_F)$. The dominant contributions in these channels come from phonon-exchange processes, so that the interactions u_F and u_B enter a regime of large attraction at low-energies. The flow of the scaling equations gives rise now to a fast growth of the $2k_F$ CDW, the $2k_F$ spin-density-wave, or the s-wave SC response function, leading to the phases shown in Fig. 1. Recalling the value of the couplings for the experimental samples, we see that the relevant region falls in this case into the phase with strong CDW correlations.

An important point in connection with the phenomenology reported in Ref. [11] is that the (3,3) nanotubes fall at low energies into a phase which is consistent

with the large diamagnetic signal observed in the experiments. This can be seen by recalling that the vector part A of the electromagnetic potential couples to the electronic current. Actually, around each Fermi point, the modes of the electron field can be arranged into a bispinor, whose hamiltonian is obtained from that of the low-energy excitations of graphene [24]:

$$H_G = \int d^2r \psi^\dagger(r) (\tau \cdot i(\nabla + A)) \psi(r) \quad (14)$$

The 1D projection to the low-energy excitations of the nanotube can be done consistently in the case of a transverse magnetic field, by choosing the vector potential as usual in the longitudinal direction of the nanotube [25]. After diagonalizing the quadratic form in (14), the 1D hamiltonian becomes

$$H_{1D} = v_F \int dk d' (k - i(\nabla + A_k(r))) \left(\begin{pmatrix} \psi_R(k) \\ \psi_L(k) \end{pmatrix} \right) \quad (15)$$

where r is the angle that supports the modulation of the longitudinal component A_k around the nanotube. It becomes clear that the vector potential couples to the charge asymmetry $\psi = \psi_R + \psi_L$.

When there is an enhanced susceptibility for the charge mismatch between left and right branches, a mechanism of screening of the magnetic field takes place, similar to the usual screening of the electric field from the total electron charge. The response function for the current χ , computed at the bosonization level, is

$$\chi_+(\omega; k) + (\omega; -k)i = \frac{1}{K_+} \frac{u_+ k^2}{\omega^2 - u_+^2 k^2} \quad (16)$$

After integration of the density fields, we obtain a contribution to the free-energy density which, in the static limit, has the form $-A_k(r)A_k(r) v_F^2 (\nabla + A)^2 = K_+ u_+$. The susceptibility (16) leads therefore to a large diamagnetic response in the regime where $1 = K_+ u_+$ diverges.

The instability in the current is triggered by the vanishing of the renormalized velocity v_{J+} at low energies. The diamagnetic response is therefore enhanced by the vanishing of K_+ and u_+ at low temperatures. The behavior of the susceptibility $v_F^2 (\nabla + A)^2 = K_+ u_+$ as a function of the temperature is actually in qualitative agreement with the divergence of the magnetic susceptibility of CN reported in Ref. [11].

We end up with a picture consistent with the experimental observations reported in Ref. [11], assuming that, as supported by the measurements of the nanotube diameter, most part of the CN contained in the zeolite matrix have preferentially a (3,3) geometry. We have seen that the transition reported in Ref. [11] may be interpreted as the breakdown of the Luttinger liquid regime, originated from the onset of phase separation into regions with opposite electronic current. As well as for graphene [25], the

existence of degenerate points in the spectrum is at the origin of the diamagnetic signal in the CN. The peculiar feature in the nanotubes is that their 1D character leads to the splitting of the electron system into regions with alternating direction of the current. This implies necessarily the appearance of domain walls in the configuration of the current. The physical picture provides then a 1D analogue of a well-known phenomenon in higher dimensions, by which the disordering effect of solitons spoils the propagation of the gauge fields. This is the role of the divergent fluctuations and consequent domain walls in the current, which lead to a phase transition in 1D as that only requires the breakdown of a discrete symmetry, namely that of the current direction in the CN.

-
- [1] L. Balents and M. P. A. Fisher, Phys. Rev. B 55, R11973 (1997).
 - [2] R. Egger and A. O. Gogolin, Phys. Rev. Lett. 79, 5082 (1997); Eur. Phys. J. B 3, 281 (1998).
 - [3] C. Kane, L. Balents and M. P. A. Fisher, Phys. Rev. Lett. 79, 5086 (1997).
 - [4] H. Yoshioka and A. A. Odintsov, Phys. Rev. Lett. 82, 374 (1999); Phys. Rev. B 59, R10457 (1999).
 - [5] M. Bockrath et al., Nature 397, 598 (1999).
 - [6] Z. Yao et al., Nature 402, 273 (1999).
 - [7] A. Yu. Kasumov et al., Science 284, 1508 (1999).
 - [8] A. F. Morpurgo et al., Science 286, 263 (1999).
 - [9] J. Gonzalez, Phys. Rev. Lett. 87, 136401 (2001).
 - [10] M. Kociak et al., Phys. Rev. Lett. 86, 2416 (2001). A. Kasumov et al., Phys. Rev. B 68, 214521 (2003).
 - [11] Z. K. Tang et al., Science 292, 2462 (2001).
 - [12] J. Gonzalez, Phys. Rev. Lett. 88, 076403 (2002); Phys. Rev. B 67, 014528 (2003).
 - [13] J. V. Alvarez and J. Gonzalez, Phys. Rev. Lett. 91, 076401 (2003).
 - [14] H. J. Liu and C. T. Chan, Phys. Rev. B 66, 115416 (2002).
 - [15] Phase separation has been also advocated in CN with dominant attractive interaction by A. De Martino and R. Egger, Phys. Rev. B 67, 235418 (2003).
 - [16] Yu. A. Krotov, D.-H. Lee and S. G. Louie, Phys. Rev. Lett. 78, 4245 (1997).
 - [17] J. Voit, Rep. Prog. Phys. 58, 977 (1995).
 - [18] The out-of-plane optical modes play a dominant role in CN of short radius, followed by in-plane optical modes and breathing modes, according to R. Bamett, E. Demler and E. Kaxiras, report cond-mat/0305006.
 - [19] A. Sedeki, L. G. Caron and C. Bourbonnais, Phys. Rev. B 65, 140515 (2002).
 - [20] D. W. Wang, A. J. Millis and S. Das Sarma, Phys. Rev. B 64, 193307 (2001).
 - [21] P. Hawrylak, G. Eliasson and J. J. Quinn, Phys. Rev. B 37, 10187 (1988).
 - [22] A. A. Nersisyan and A. M. Tsvelik, Phys. Rev. B 68,

235419 (2003).

[23] K. Kamide et al., Phys. Rev. B 68, 024506 (2003).

[24] J. Gonzalez, F. Guinea and M. A. H. Vozmediano, Nucl. Phys. B 424, 595 (1994).

[25] R. Saito, G. Dresselhaus and M. S. Dresselhaus, Physical Properties of Carbon Nanotubes, Chap. 6, Imperial College Press, London (1998).